第32卷第12期 焊 接 学 报 Vol. 32 No. 12
2011年12月 TRANSACTIONS OF THE CHINA WELDING INSTITUTION December 2011

AZ31B合金热化学反应热喷涂复相陶瓷涂层制备及性能

马 壮，邹积峰，王 伟，李智超
(辽宁工程技术大学 材料加工与表面技术研究所，阜新 123000)

摘 要：采用机械球磨和PVA(聚乙烯醇)造粒制成喷涂复合粉末，采用热化学反应火焰喷涂技术，在镁合金AZ31B表面制备Al_2O_3基复相陶瓷涂层. 利用X射线衍射(XRD)、扫描电镜(SEM)分析了喷涂复合粉末和复合陶瓷涂层的组成及形貌，并对涂层的热震性能、致密性、显微硬度和耐磨性进行测试. 结果表明，复合粉末经12 h球磨后有化学反应发生，造粒后形成相互包覆的球状结构. 在制备涂层过程中伴随热化学反应的发生，涂层中生成$Al_{3.21}Si_{0.47}$，$MgAl_2O_4$，$Mg_{3.5}Al_9Si_{1.5}O_{20}$等新相. 该复合涂层熔化较充分，涂层与基体结合紧密，界面处Mg元素有明显扩散. 复合涂层热震可达40次，与相同条件下，双层陶瓷涂层提高了近一倍，孔隙率为15.1%，最大显微硬度值可达到1 016 HV0.1. 涂层热震性能、致密性、显微硬度和耐磨性明显优于普通热喷涂陶瓷涂层.

关键词：镁合金；热化学反应热喷涂；陶瓷涂层；性能
中图分类号：TG174.4 **文献标识码**：A **文章编号**：0253－360X(2011)12－0046－05

马 壮

0 序 言

近年来热化学反应法制备陶瓷涂层引起了广泛的关注. 该方法以料浆法为基础，增添热固化环节，在热固化过程中，金属与陶瓷涂层界面处可发生热化学反应产生新的陶瓷相，从而提高界面强度、改善涂层性能[1,2]. 但是这种方法制备陶瓷涂层周期较长，效率较低. 文中采用热喷涂法取代涂覆法，以热喷涂热量代替固化加热过程，以达到热化学反应的目的，称其“热化学反应热喷涂法”[3]. 这种技术工序少、制备效率高，涂层内部及涂层间存在化学反应并形成化学结合，打破热喷涂层单一的机械结合方式，提高了涂层的结合性能.

试验采用热化学反应热喷涂技术，将球磨、造粒后制得的陶瓷粉末用火焰喷涂的方法在镁合金AZ31B表面制备复相陶瓷涂层，并与普通陶瓷涂层进行结构、性能对比分析.

1 试验方法

基体材料为AZ31B，尺寸为20 mm×20 mm×7 mm. 试验所用喷涂材料为高纯度陶瓷粉末Al_2O_3，TiO_2，ZnO，SiO_2及铝粉，按55% Al_2O_3-9% TiO_2-8% ZnO-9% SiO_2-19% Al(质量分数)混合. Al_2O_3-TiO_2涂层具有耐磨、耐蚀、耐热、绝缘等优良性能，是目前广泛使用的Al_2O_3基陶瓷涂层[4,5]. SiO_2和ZnO的加入可使混合后的陶瓷粉末在喷涂过程中发生热化学反应并形成新的陶瓷相，有利于提高涂层的性能[6-8]. 铝粉的加入为体系提供了良好的液相传质条件，可以促进喷涂团聚粉在飞行燃烧中的反应，增加喷涂粒子的熔化程度，因而对提高涂层与基体的结合强度具有重要意义. 为更好地探讨热化学反应热喷涂中涂层质量和性能，试验也制备了喷涂材料为Al_2O_3 + 13% TiO_2普通喷涂试样以进行对比试验.

喷涂材料制备过程：陶瓷粉末过筛→配料→混合球磨→混合粉末200 ℃烘干→聚乙烯醇(PVA)造粒→团聚粉末破碎后过筛→复合陶瓷粉末. 采用QM-1SP2型行星式球磨机进行干法球磨，球料比为5∶1，球磨时间12 h，旋转频率512 r/min；粘结剂为7%(质量分数)的聚乙烯醇水溶液，与骨料1∶5混合.

试样制备过程：AZ31B基体喷砂粗化→喷涂80% Ni-20% Al过渡层(质量分数)→喷涂复合陶瓷涂层→置入200 ℃炉内随炉缓慢冷却. 在喷前先喷

收稿日期：2010－10－20
基金项目：辽宁省教育厅创新团队基金项目(2009T044)

一层 Ni-Al 过渡层,既可起到防止基体熔化的作用,还可降低因镁合金基体与涂层线膨胀系数差异而引起的热应力. 采用 QT-E2000-7/H 型两用火焰喷枪喷涂过渡层和陶瓷涂层,喷涂工艺参数见表 1.

表 1　喷涂工艺参数

Table 1　Spraying parameters

涂层	氧气压力 p_1/MPa	乙炔压力 p_2/MPa	预热温度 T/℃	移动速度 v/(mm·s^{-1})	喷距 l/mm	送粉量 q/(kg·h^{-1})
Ni-Al 层	0.8 ~ 0.9	0.11 ~ 0.14	300 ~ 400	60 ~ 90	110 ~ 160	0.9 ~ 1.2
陶瓷涂层	0.8 ~ 0.9	0.11 ~ 0.14	350 ~ 450	60 ~ 90	110 ~ 160	1.0 ~ 1.5

涂层热震试验是将试样整体放入 400 ℃电阻炉中保温 15 min 后迅速取出水淬,如此循环下去,直至涂层出现裂纹或剥落,用循环次数表征涂层的抗热震性; 用浮力法测试涂层孔隙率以评定其致密性. 磨粒磨损在 ML-10 型盘销式磨粒磨损试验机上进行试验,试验参数: 外加载荷 20 N,对磨材料 4 号金相砂纸,磨损行程为 80 mm,往返 3 次,旋转频率 60 r/min. 使用日本岛津 SSX-550 附带能谱分析仪(EDS)扫描电镜观察喷涂粉末及试样的表面和界面形貌; 采用日本理学 D/MAX-RB 型 X 射线衍射仪分析复合陶瓷涂层相结构. 采用 HVS-1000 型数字式显微硬度计测试陶瓷涂层的显微硬度,载荷 1 N,加载时间 10 s.

2　试验结果与讨论

2.1　复合粉末形貌及物相分析

图 1 为复合粉末经 12 h 球磨后的 SEM 形貌及 XRD 图谱. 由图 1a 可以看出,复合粉末在机械力的作用下,发生了塑性变形,呈明显的层片状和颗粒状,颗粒周围附着有片状微小颗粒,这可能是由于粉末中的延展性成分(铝粉)在球磨过程中发生塑性变形和加工硬化,随球磨的进行,颗粒破碎成细小层状颗粒. 另外,粉末有较明显的团聚现象,分布不均匀. 图 1b XRD 分析表明,复合粉末在球磨后有 $Al_{3.21}Si_{0.47}$,$Zn_{1.9}SiO_4$ 等新相生成,说明复合粉末在机械力的作用下发生了化学反应.

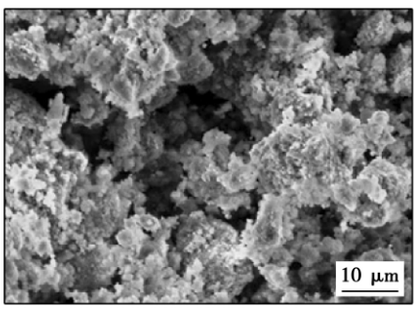

(a) 复合粉末12 h球磨后SEM形貌

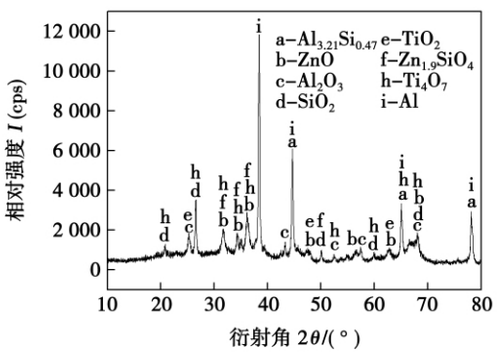

(b) 复合粉末球磨后XRD图谱

图 1　球磨后复合粉末 SEM 形貌及 XRD 图谱

Fig. 1　SEM images and XRD patterns of composite powders after 12h ball milling

图 2 为复合粉末造粒后的 SEM 形貌. 由图 2 可以看出,造粒后的粉末主要呈球状,颗粒的包覆效果极为显著,表面有絮状附着物,这是因为聚乙烯醇溶液与球磨后的复合粉末混合后使不同物性的颗粒粘结在一起[9],达到了相互包覆的结构,增加了粉末的流动性,有利于喷涂过程中粉末的充分熔融并发生热化学反应,形成高质量的陶瓷涂层.

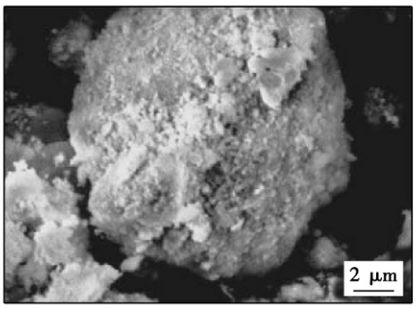

图 2　造粒后复合粉末 SEM 形貌

Fig. 2　SEM images of composite powders after granulation

2.2　陶瓷涂层物相分析

图 3 为陶瓷涂层 XRD 图谱. 由图 3a 可以看出,普通热喷涂层除原有的陶瓷粒子外,还有 Al_3Ti

等物质生成，其组成物来源于陶瓷粉末内部的反应生成的中间产物. 由图 3b 可以看出，热化学反应热喷涂层本身除了含有 Al_2O_3，TiO_2，ZnO 外，还有 $Al_{3.21}Si_{0.47}$，$MgAl_2O_4$，$Mg_{3.5}Al_9Si_{1.5}O_{20}$等新相.

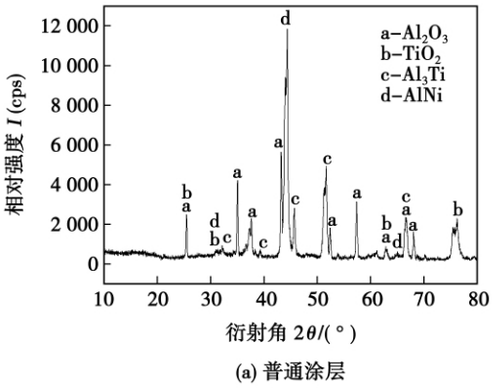

(a) 普通涂层

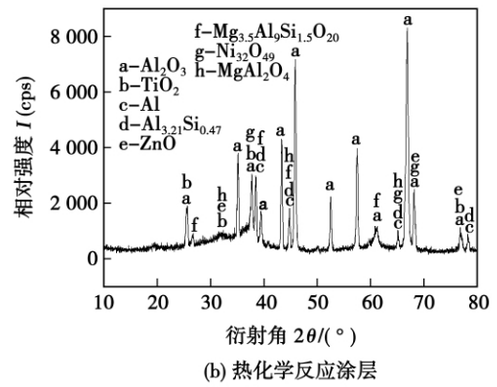

(b) 热化学反应涂层

图 3 陶瓷涂层 XRD 图谱

Fig. 3 XRD patterns of coatings

2.3 陶瓷涂层表面及界面特征分析

图 4 为普通热喷涂和热化学反应热喷涂陶瓷涂层表面及界面 SEM 形貌. 由图 4a 和图 4c 可见，普通热喷涂层有较多未熔化的陶瓷颗粒，孔隙较多，界面处结合不紧密，涂层结构较为疏松，这可能是因为喷涂过程中陶瓷粒子熔化不充分所致. 由图 4b 和图 4d 所示，热化学反应热喷涂层大部分区域比较平滑，未熔化的颗粒很少，说明喷涂材料在喷涂过程中熔融较为充分. 涂层与 Ni–Al 过渡层之间界线不明显，说明涂层与 Ni–Al 过渡层已熔为一体，结合牢靠.

图 5 为涂层能谱线扫描分析. 由图 5a 可以看出，基体元素和涂层各元素扩散不明显. 普通热喷涂由于喷涂时间极短，火焰温度较低，因而形成涂层过程中只发生物理过程，扩散现象并不明显. 由图 5b 可以看出，基体元素和涂层各元素都有不同程度的轻微扩散，其中 Mg 元素的扩散较为明显. 这是由于喷涂过程中发生热化学反应，改变了原有的物相组成、组织结构及涂层的聚合方式. 由于基体与涂层界面处有新相产生，因此也表现出一定程度的化学结合，因此涂层主要的结合方式除了机械结合外，还有化学冶金结合.

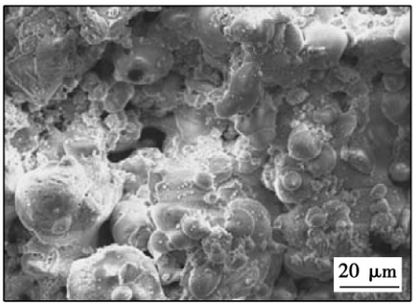

(a) 普通热喷涂层表面形貌

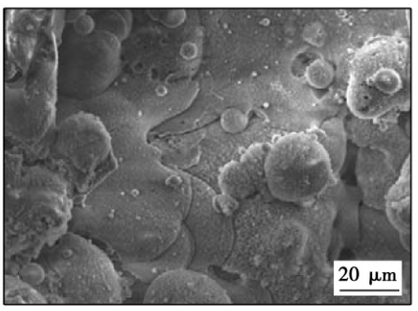

(b) 热化学反应热喷涂层表面形貌

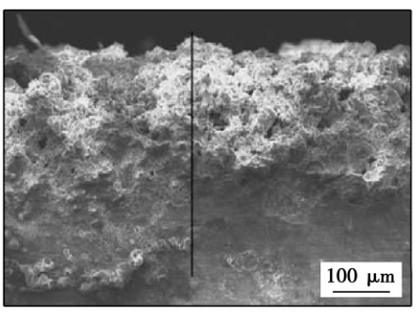

(c) 普通热喷涂层界面形貌

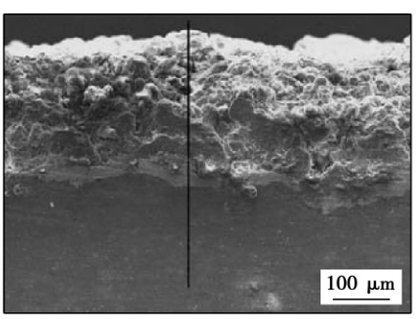

(d) 热化学反应热喷涂层界面形貌

图 4 陶瓷涂层形貌

Fig. 4 SEM images of ceramic coatings

2.4 涂层热震性能及致密性

热化学反应涂层的热震性能和致密性明显好于普通热喷涂陶瓷涂层. 普通热喷涂涂层热震 23 次，涂层脱落严重，孔隙率为 18.5%. 而热化学反应热

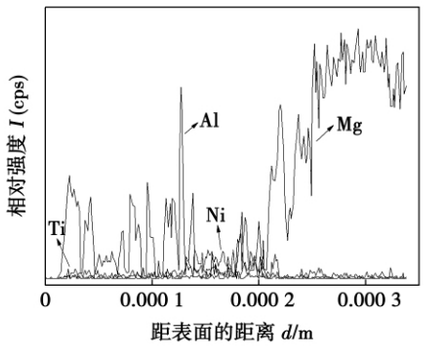

(a) 普通热喷涂层能谱线扫描

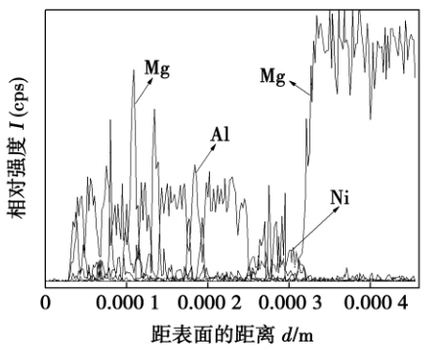

(b) 热化学反应热喷涂层能谱线扫描

图 5　涂层能谱线扫描分析

Fig. 5　Cross-section line energy spectrum analysis of coatings

喷涂层经 40 次热冲击循环涂层结合良好，无脱落现象. 热化学反应热喷涂涂层，孔隙率可达 15.1%.

2.5　涂层界面区硬度分布

两种涂层和基体显微硬度分布曲线如图 6 所示. 可以看出，镁合金基体的显微硬度值约为 65 HV0.1，普通热喷涂层最大显微硬度值可达到 616 HV0.1，与镁合金基体相比，提高了 8.5 倍. 热化学反应热喷涂层最大显微硬度值可达到 1 016 HV0.1，比普通热喷涂提高 400 HV0.1，这是因为涂层的硬度与涂层本身的物相组成、组织结构、涂层本身的聚合强度、致密性密切相关. 热化学反应热喷涂层中除机械结合外，还形成化学冶金结合，组织结构更为致密，涂层聚合强度高，因此热化学反应热喷涂层具有较高的硬度值.

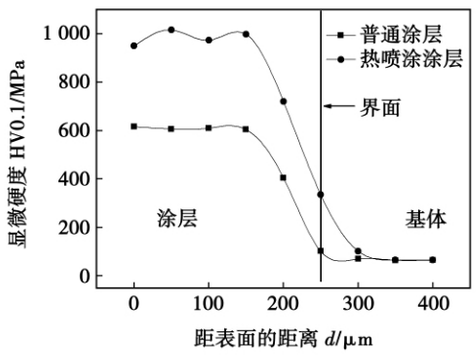

图 6　涂层和基体的显微硬度分布

Fig. 6　Distribution curves of microhardness of coating and substrate

2.6　陶瓷涂层耐磨性

图 7 为各涂层和基体单位面积磨损量随滑动距离变化的关系曲线. 可以看出，镁合金基体在 20 N 载荷下单位面积磨损量远高于喷涂试样. 热化学反应热喷涂陶瓷涂层的磨损量明显小于普通热喷涂陶瓷涂层，显示出较好的耐磨性. 这是因为涂层中生成了较多的硬质相，涂层致密均匀，结合强度较高.

图8为两种热喷涂层磨损表面形貌. 由图8 a

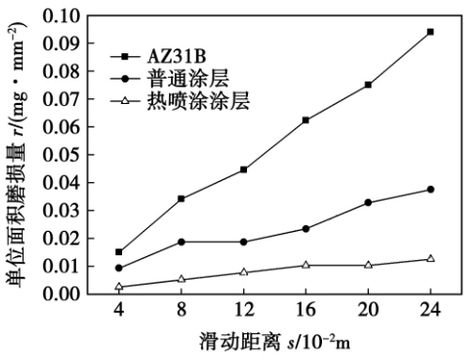

图 7　涂层和基体磨损量随滑动距离变化的关系曲线

Fig. 7　Substrate and coatings comparison diagram

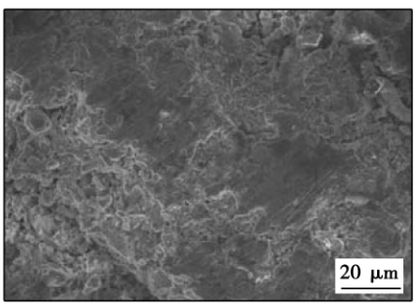

(a) 普通热喷涂层磨损形貌

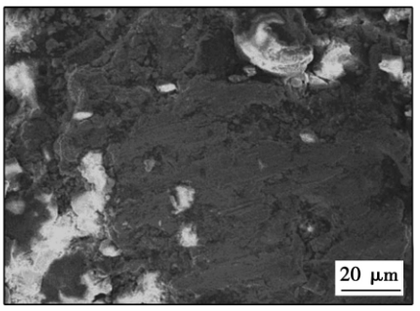

(b) 热化学反应热喷涂层磨损形貌

图 8　陶瓷涂层磨损形貌

Fig. 8　Wear images of ceramic coatings

可以看出，普通涂层磨损表面相当粗糙，出现大面积的剥落，有较多磨损碎片剥落后留下的凹坑，这主要是因为普通涂层存在很多孔隙，极易引起应力集中进而发展成为裂纹源，陶瓷材料本身的断裂韧性较差，裂纹极易扩展，最终导致涂层材料的脱落，其磨损机制主要为断裂破坏机制. 由图8b可以看出，热化学反应热喷涂层表面较为平整，没有明显的划痕，涂层剥落很少，这主要与涂层本身的结构，结合强度以及致密性等因素有关.

3 结 论

(1) 喷涂原始复合粉末经12 h机械球磨后发生了塑性变形，呈明显的层片状和颗粒状，XRD分析有 $Al_{3.21}Si_{0.47}$，$Zn_{1.9}SiO_4$ 等新相生成，说明复合粉末在机械力的作用下已发生了化学反应.

(2) 采用热化学反应喷涂法制备了复合陶瓷涂层. 在喷涂过程中有热化学反应发生，涂层中有 $Al_{3.21}Si_{0.47}$，$MgAl_2O_4$，$Mg_{3.5}Al_9Si_{1.5}O_{20}$ 等新相. 涂层表面熔化较充分，涂层与基体结合紧密，Mg元素有明显扩散.

(3) 热化学反应热喷涂陶瓷涂层最大显微硬度值可达到1 016 HV0.1，比普通热喷涂提高400 HV0.1，与镁合金基体相比，提高了8.5倍. 热化学反应热喷涂陶瓷涂层抗热震性和致密性明显优于普通热喷涂层，热震次数可达到40次，孔隙率为15.1%. 涂层磨损后表面较为平整，没有明显的划痕，涂层剥落很少，其磨损机制主要为断裂破坏机制.

参考文献:

[1] 李浩群，邵天敏，杨 政，等. 铝合金基体上 Al_2O_3 基陶瓷涂层形成机理[J]. 清华大学学报(自然科学版)，2000，40(4)：92－95.
Li Haoqun，Shao Tianmin，Yang Zheng，*et al*. Formation mechanism for Al_2O_3-based ceramic coatings on aluminum alloy substrates[J]. Journal of Tsinghua University (Science and Technology)，2000，40(4)：92－95.

[2] Yan Dianran，He Jining，Wu Jianjun，*et al*. The corrosion behavior of plasma spray Al_2O_3 ceromics coating in dilute HCl solution[J]. Surface and Coating Technology，1997，8(9)：191－195.

[3] 马 壮，曲文超，李智超，等. 热化学反应喷涂 Al_2O_3 基复合陶瓷涂层的制备及其性能[J]. 中国有色金属学报，2009，19(6)：1093－1099.
Ma Zhuang，Qu Wenchao，Li Zhichao，*et al*. Preparation and properties of Al_2O_3 based composite ceramic coating on pure copper surface by thermo-chemical reaction spraying[J]. The Chinese Journal of Nonferrous Metals，2009，19(6)：1093－1099.

[4] 卢金斌，梁 存，彭竹琴，等. 等离子弧熔覆添加 $Al_2O_3+TiO_2$ 铁基合金涂层组织和耐磨性[J]. 焊接学报，2008，29(12)：33－36.
Lu Jinbin，Liang Cun，Peng Zhuqin，*et al*. Microstructure and wear resistance of plasma cladding $Al_2O_3+TiO_2$/Fe alloy composite coating[J]. Transactions of the China Welding Institution，2008，29(12)：33－36.

[5] 雷阿利，徐大鹏，冯拉俊，等. 热喷涂法制备的 La^{3+} 掺杂纳米 TiO_2 粉末的表征[J]. 焊接学报，2008，29(8)：25－28.
Lei Ali，Xu Dapeng，Feng Lajun，*et al*. Characterization of La^{3+} doped TiO_2 prepared by plasma spraying[J]. Transactions of the China Welding Institution，2008，29(8)：25－28.

[6] 李春福，王 斌，王 戎，等. 纳米掺杂 Al_2O_3/ZrO_2 等离子喷涂涂层的组织及性能[J]. 中国有色金属学报，2007，17(9)：1397－1403.
Li Chunfu，Wang Bin，Wang Rong，*et al*. Microstructure and performance of nano-doping Al_2O_3/ZrO_2 plasma spray coatings[J]. The Chinese Journal of Nonferrous Metals，2007，17(9)：1397－1403.

[7] Ramaswany A，Seetharamu S，Varma K B R. Al_2O_3-ZrO_2 composite coatings for thermal-barrier application[J]. Composites Science and Technology，1997，57：81－89.

[8] 李慕勤，马 臣，谭 伟，等. SiO_2 添加剂对 $8\%Y_2O_3$ 稳定的 ZrO_2 涂层热震前后表面形貌的影响[J]. 焊接学报，2003，24(3)：59－60，64.
Li Muqin，Ma Chen，Tan Wei，*et al*. Influence of additive SiO_2 on stable $ZrO_2+8\%Y_2O_3$ coatings of thermal shock[J]. Transactions of the China Welding Institution，2003，24(3)：59－60，64.

[9] 程汉池，栗卓新，汤春天. 喷雾造粒在热喷涂中的应用研究[J]. 中国化工装备，2005，7(4)：18－23.
Cheng Hanchi，Li Zhuoxin，Tang Chuntian. Research on applications of spray granulation in thermal spraying[J]. China Chemical Industry Equipment，2005，7(4)：18－23.

作者简介: 马 壮，男，1963年出生，教授，博士研究生导师. 主要从事金属材料及表面改性技术研究工作. 发表论文60余篇. Email：mazh123@263.net

metal; microstructure; brazing mechanism

Interfacial characteristics of welded joint between aluminum alloy and stainless steel by resistance spot welding QIU Ranfeng[1,2], YU Hua[1], SHI Hongxin[1], ZHAN Keke[1], TU Yimin[1], SATONAKA Shinobu[3] (1. School of Materials Science and Engineering, Henan University of Science and Technology, Luoyang 471003, China; 2. Henan Key Laboratory of Advanced Non-ferrous Metals, Luoyang 471003, China; 3. Graduate School of Science and Technology, Kumamoto University, Kurokami 2-39-1, Kumamoto 860-8555, Japan). p 37 - 40

Abstract: Aluminum alloy A5052 and stainless steel SUS304 were welded by resistance spot welding with a cover plate. The welding interface region of the joint was observed with electron microscopy, and the microstructure and distribution of the reaction products were analyzed as well. The results reveal that a serration reaction layer consisting of Fe_2Al_5 and $FeAl_3$ forms in the welding interface and the reaction layer thickness varies with the welding current and the position at the welding interface. Moreover, the reaction blocks in aluminum alloy near the welding interface were observed, which were estimated as a hexagonal AlFeCr having $a = 2.451$ nm and $c = 0.758$ nm based on analysis of selected area electron diffraction patterns.

Key words: aluminum alloy; stainless steel; resistance spot welding; interface reaction layer

Study on cold metal transfer welded lap joints of Mg/Al dissimilar metals SHANG Jing[1], WANG Kehong[1], TIAN Hongjun[2], ZHOU Qi[1], LI Guangle[1] (1. School of Material Science and Engineering, Nanjing University of Science and Technology, Nanjing 210094, China; 2. State-owned 5103 Factory, Nanzhao 474650, China). p 41 - 45

Abstract: AZ31B magnesium alloy and 6061 aluminum alloy were welded by cold metal transfer (CMT) welding method with pure copper (HS201) as the filler metal. Shear strength and micro-hardness of the lap joint were tested. The microstructure and fracture morphology of joint were studied by means of scanning electron microscope (SEM) and energy dispersive X-ray (EDX). The results showed that good weld with the highest shear bonding strength of 27.9MPa was obtained under the welding current of 109 A, welding voltage of 10.9 V, wire feed speed of 4.9 mm/s, welding speed of 0.45 m/min. Intermetallic compounds of Mg_2Cu and $MgCu_2$ were formed in the Mg-Cu side where was oxidized. Al-Cu-Mg ternary intermetallic compounds and Al_2Cu were formed on the Al-Cu side. Micro-hardness in both sides of fusion zone was suddenly increased due to intermetallic compounds. Maximum micro-hardness of Al-Cu side and Mg-Cu side were 242 HV and 347 HV respectively. The fracture occurred in the fusion zone of Mg side, and fracture nature was brittle fracture. Oxidation in the welding process and plenty of intermetallic compounds distributed continuously in the fusion zone, and resulted in the fracture.

Key words: cold metal transfer welding; aluminum alloy; magnesium alloy; dissimilar metals welding; intermetallic compounds

Preparation and properties of composite ceramic coating on AZ31B alloy by thermo-chemical reaction spraying MA Zhuang, ZOU Jifeng, WANG Wei, LI Zhichao (Institute of Materials Processing and Surface Technology, Liaoning Technical University, Fuxin 123000, China). p 46 - 50

Abstract: The spraying composite powder was prepared by mechanical ball milling and polyvinyl alcohol (PVA) granulation. Al_2O_3-based composite ceramic coating was prepared on the surface of magnesium alloy AZ31B by thermo-chemical reaction spraying. XRD and SEM were used to analyze the composition and morphology of the spraying composite powder and composite ceramic coating. The thermal shock, compactness, microhardness and wear properties of the composite ceramic coating were investigated respectively. The results showed that chemical reaction had happened in composite powder after 12 hours ball milling and globular structure coated each other was formed after granulation. Thermo-chemical reaction was carried out in the process of preparing coatings. New phase such as $Al_{3.21}Si_{0.47}$, $MgAl_2O_4$ and $Mg_{3.5}Al_9Si_{1.5}O_{20}$ were found in the coating. The melting rate of composite ceramic coating was high and the combination of the coating and matrix was good. Mg element took place remarkable diffusion in the interface of composite coating. The thermal-shock times of this coating was 40, the porosity was 15.1% and the maximum microhardness value reached $HV_{0.1}$ 1016. The thermal shock, compactness, microhardness and wear properties of this coating was significantly better than the ones with common spraying coating.

Key words: magnesium alloy; thermo-chemical reaction spraying; ceramic coating; performance

Influence of gas shroud on property of plasma sprayed thermal barrier coating WEI Qi, LI Hui, LI Hong, ZHANG Linwei (College of Materials Science and Engineering, Beijing University of Technology, Beijing 100124, China). p 51 - 54

Abstract: The comparative study were carried out on the microstructure as well as the properties of the coating prepared by atmospheric plasma spraying and shroud plasma spraying. The results showed that, compared to the conventional atmospheric plasma sprayed (APS) coating, the shroud plasma sprayed (SPS) coating contained less unmelted or partially melted particles and oxide content, and porosity was lower. The SPS coating presented superior oxidation resistance at 1 080 ℃ than the APS one. The reason owed to the mitigation of the involvement of the surrounding air that caused turbulent of the plasma, consequently, the particles were more fully melted and less oxide formed in the coating. The finally deposited SPS coating was denser and contained more Al element, which induced the formation of compact Al_2O_3 layer at the early stage of oxidation. This compact Al_2O_3 layer would slow down the thickening rate of thermally grown oxide (TGO) that provides better resistance to the bond layer, therefore the SPS coating presents higher resistance to high temperature oxidation.

Key words: plasma spray; thermal barrier coating; oxidation resistance

Influence of welding sequence on welding residual stress distribution in thick plate joint DENG Dean[1], SHOICHI Kiyoshima[2] (1. College of Materials Science and Engineering, Chongqing University, Chongqing 400045, China; 2. Research Center of Computational Mechanics, Inc., Tokyo 142-0041, Japan). p 55 - 58

Abstract: Features of welding residual stress distribution in an austenitic stainless steel thick plate joint were investigated by means of experiment and numerical simulation technology.